Electronic Supplementary Information

Inclusion Complexes of Fullerenes with Flexible Tetrathiafulvalene Derivatives Bearing Four Aryls through the Sulfur Bridges

Jibin Sun,[a] Xiaofeng Lu,[a] Manabu Ishikawa,[b] Yoshiaki Nakano,[b] Shangxi Zhang,[a] Jinlian Zhao,[a] Yongliang Shao,[a] Zhaohui Wang,[c] Hideki Yamochi,[b] and Xiangfeng Shao[a]*

[a] *State Key Laboratory of Applied Organic Chemistry, Lanzhou University, Tianshui Southern Road 222, Lanzhou 730000, Gansu Province, P. R. China*

[b] *Research Centre for Low Temperature and Materials Sciences, Kyoto University, Sakyo-ku, Kyoto 606-8501, Japan*

[c] *Key Laboratory of Organic Solids, Institute of Chemistry, Chinese Academy of Science, Beijing 100089, P. R. China*

Email: shaoxf@lzu.edu.cn (X. S.)

Experimental

Chlorobenzene (PhCl) and carbon disulfide (CS_2) were distilled over P_2O_5 under inert condition and stored in the long-necked flask under the argon atmosphere. **TTF1**–**TTF3** were prepared according to the method reported in the literature,[1] and further purified by recrystallization from CH_2Cl_2/*n*-hexane to give red crystalline samples. $\mathbf{C_{60}}$ and $\mathbf{C_{70}}$ were purchased from J&K chemicals (Beijing), and further purified by recrystallization from toluene.

Complex **TTF1**•$\mathbf{C_{60}}$•$\mathbf{CS_2}$ was prepared by slow evaporation of the mixed solution of **TTF1** and $\mathbf{C_{60}}$ in CS_2 at room temperature (RT). After 5 days, the black platelet single crystals were formed. Complex **TTF2**•$\mathbf{C_{60}}$ was prepared by slow evaporation of the mixed solution of **TTF2** and $\mathbf{C_{60}}$ in PhCl at RT. After 20 days, the black platelet single crystals were formed. **TTF3**•$(\mathbf{C_{70}})_2$•$(\mathbf{PhCl})_2$ were prepared by slowly evaporation of the mixed solution of **TTF3** and $\mathbf{C_{70}}$ in PhCl at RT. After 20 days, the black platelet single crystals were formed.

Table S1. Experimental conditions for the preparation of inclusion complexes

TTF	Fullerene	Solvent	Complex	Appearance
TTF1, 34.1 mg	$\mathbf{C_{60}}$, 14.4 mg	$\mathbf{CS_2}$, 14 mL	**TTF1**•$\mathbf{C_{60}}$•$\mathbf{CS_2}$, 29.2 mg	Black block
TTF2, 6.9 mg	$\mathbf{C_{60}}$, 14.4 mg	**PhCl**, 14 mL	**TTF2**•$\mathbf{C_{60}}$, 8.2 mg	Black plates
TTF3, 13.8 mg	$\mathbf{C_{70}}$, 8.4 mg	**PhCl**, 10 mL	**TTF3**•$(\mathbf{C_{70}})_2$•$(\mathbf{PhCl})_2$, 6.0 mg	Black prism

The X-ray diffraction measurement was carried out on SuperNova (Agilent) type diffractometer. The crystal structures of complexes **TTF1**•$\mathbf{C_{60}}$•$\mathbf{CS_2}$, **TTF2**•$\mathbf{C_{60}}$, and **TTF3**•$(\mathbf{C_{70}})_2$•$(\mathbf{PhCl})_2$ were solved by a direct method *SIR2004*[2] and refined by full-matrix least-squares method on F^2 by means of *SHELXL-97*.[3] The calculated positions of the hydrogen atoms were included in the final refinement. The selected crystallographic data are summarized in Table S2. The UV-vis spectra in chlorobenzene (PhCl) solution (10^{-4} mol L^{-1}) were measured at 20 ^{o}C on Lambda 950 spectrometer (PerkinElmer). The absorption spectra were measured on the solid state by dispersing the complexes on the KBr pellet. The infrared (IR) spectra (400–7500 cm^{-1}) were record on the PerkinElmer Spectrum 400 spectrometer with the resolution of 2 cm^{-1}. The UV-vis-NIR in KBr (3800–42000 cm^{-1}) were recorded on the PerkinElmer Lambda1050 spectrometer.

Table S2. Selected crystallographic data for complexes **TTF1•C_{60}•CS_2**, **TTF2•C_{60}**, and **TTF3•$(C_{70})_2$•$(PhCl)_2$**.

	TTF1•C_{60}•CS_2	**TTF2•C_{60}**	**TTF3•$(C_{70})_2$•$(PhCl)_2$**
CCDC number	986605	986606	986607
Empirical formula	$C_{95}H_{28}O_4S_{10}$	$C_{94}H_{28}S_8$	$C_{186}H_{38}Cl_2S_8$
Formula weight	1553.77	1413.64	2599.54
Temperature [K]	113(2)	113(2)	100(2)
λ [Å]	0.71075	0.71075	0.71075
Crystal size [mm^3]	0.35×0.27×0.10	0.32×0.10×0.06	0.43×0.14×0.06
Crystal system	triclinic	triclinic	monoclinic
space group	$P\bar{1}$	$P\bar{1}$	$P2_1/c$
a [Å]	10.283(4)	10.346(8)	21.567(2)
b [Å]	10.340(4)	10.452(9)	21.385(2)
c [Å]	16.018(7)	13.714(12)	45.525(4)
α [°]	103.299(5)	88.75(3)	90
β [°]	104.031(5)	86.12(3)	90.307(1)
γ [°]	100.895(7)	79.37(3)	90
V [$Å^3$]	1553(1)	1454(2)	20996(3)
Z	1	1	8
d_{calc} [$g·cm^{-3}$]	1.661	1.614	1.645
μ [mm^{-1}]	0.42	0.368	0.296
$2\theta_{max}$ [°]	55.72	55.92	58.60
Data/restraints/parameters	4845/0/494	3788/0/461	51781/0/3529
GooF	0.981	0.994	1.097
R [$I > 2\sigma(I)$]	0.043	0.074	0.082
wR_2	0.1177	0.1652	0.1793

References

[1] a) J. Sun, X. Lu, J. Shao, X. Li, S. Zhang, B. Wang, J. Zhao, Y. Shao, R. Fang, Z. Wang, W. Yu and X. Shao, *Chem. Eur. J.,* 2013, **19**, 12517. b) J. Sun, X. Lu, J. Shao, Z. Cui, Y. Shao, G. Jiang, W. Yu and X. Shao, *RSC Adv.,* 2013, **3**, 10193

[2] M. C. Burla, R. Caliandro, M. Camalli, B. Carrozzini, G. L. Cascarano, L. de Caro, C. Giacovazzo, G. Polidori and R. Spagna, *J. Appl. Cryst.,* 2005, **38**, 381–388.

[3] G. M. Sheldrick, *SHELXL-97, A Program for Crystal Structure Refinement.* University of Göttingen, Göttingen, Germany, 1997.

Crystal structures

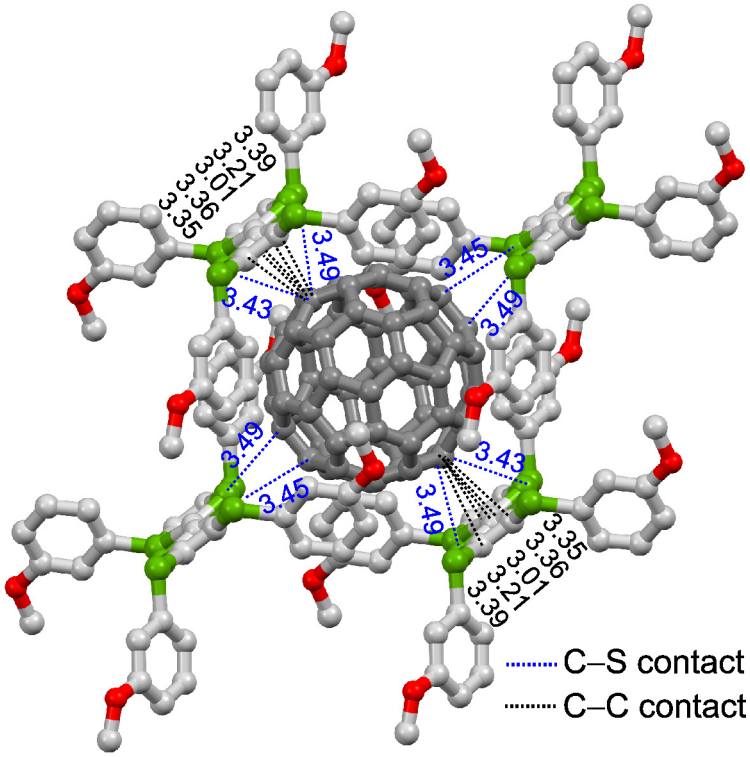

Fig. S1 Intermolecular atomic short contacts (blue and black dashed lines for C-S and C-C contacts respectively) between **TTF1** and C_{60} in **TTF1•C_{60}•CS_2**. The C–C atomic short contacts between the aryls and C_{60} are also observed: 3.27, 3.32, 3.37, and 3.38 Å.

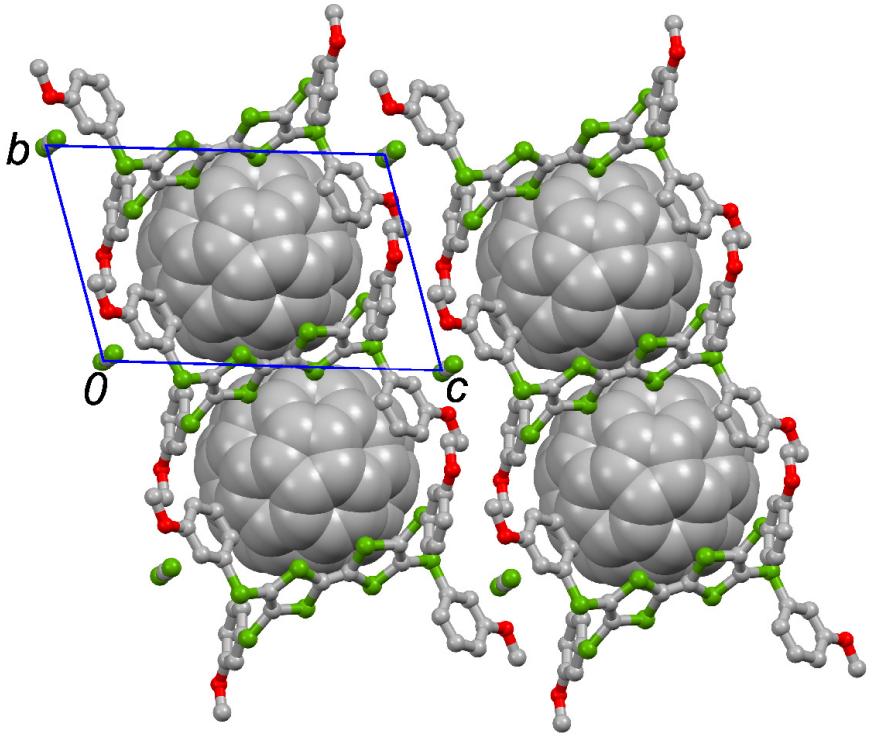

Fig. S2 Crystal structure of **TTF1•C_{60}•CS_2** projected along the *a*-axis.

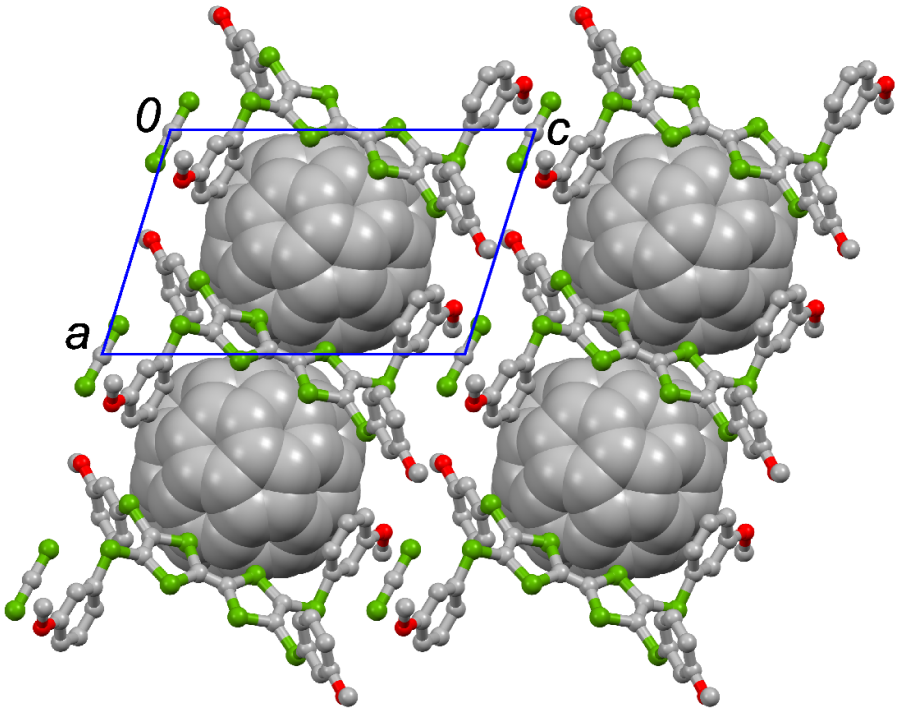

Fig. S3 Crystal structure of **TTF1•C_{60}•CS_2** projected along the *b*-axis.

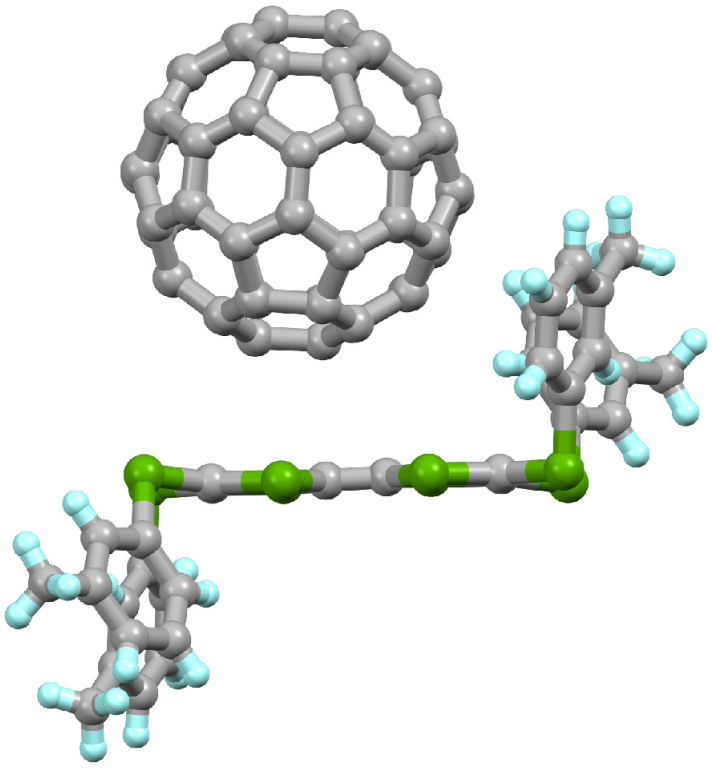

Fig. S4 Unit cell contents of **TTF2•C_{60}** viewed along the short axis of **TTF2**. The grey, green, and cyan balls represent carbon, sulfur, and hydrogen atoms, respectively. The asymmetric unit contains ½ **C_{60}** and ½ **TTF2**. The centers of **C_{60}** and **TTF2** molecules are located at (0.5, 0.5, 0.5) and (0, 0, 0.5) respectively. Thus, the **C_{60}** molecule is encapsulated by four **TTF2** molecules.

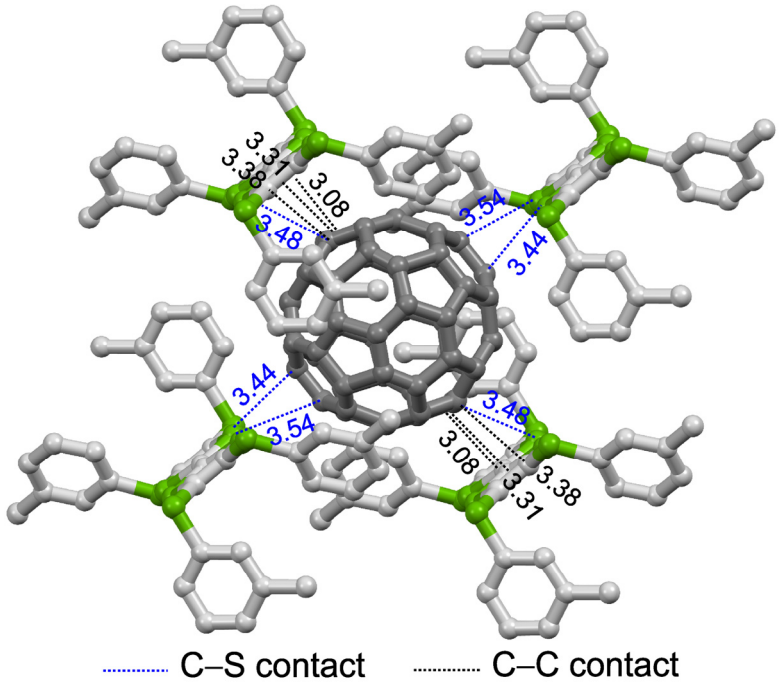

Fig. S5 Intermolecular atomic short contacts (blue and black dashed lines for C-S and C-C contacts respectively) between central core of **TTF2** and **C_{60}** in **TTF2•C_{60}**. The C–C atomic short contacts are also observed between the aryls and C_{60}: 3.27 and 3.38 Å. The grey and green balls represent carbon and sulfur atoms respectively, and the hydrogen atoms are omitted for clarity.

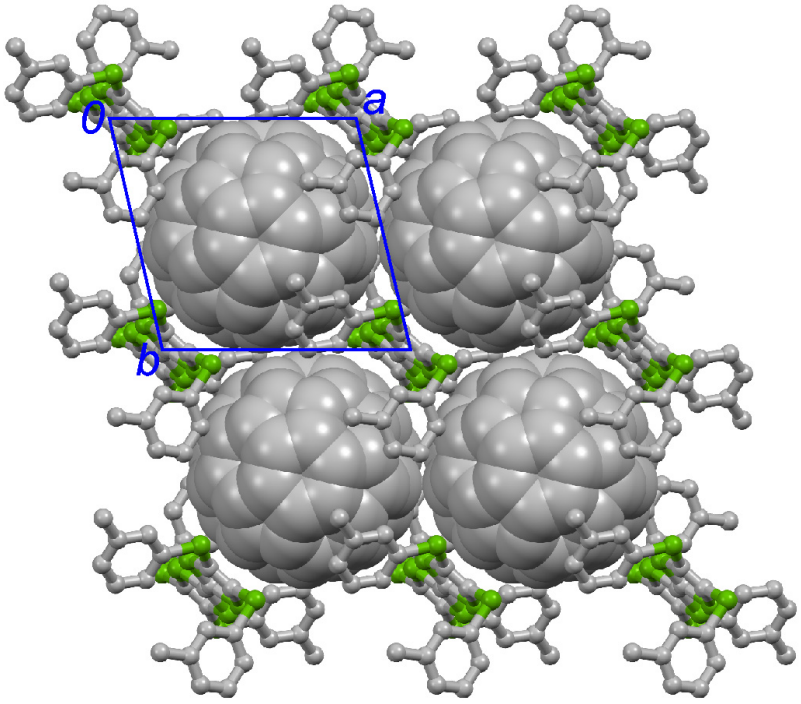

Fig. S6 Crystal structure of **TTF2•C_{60}** projected along the crystallographic *c*-axis with hydrogen atoms omitted for clarity. The centre-to-centre distances between neighbouring **C_{60}** molecules along the *a*- and *b*-axes are 10.35 and 10.45 Å respectively.

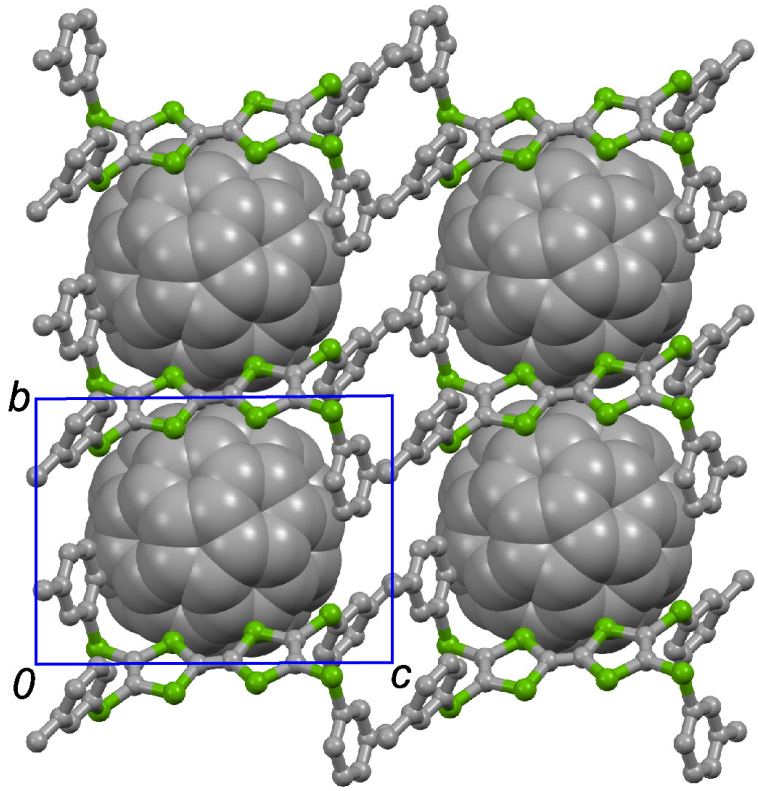

Fig. S7 Crystal structure of **TTF2•C_{60}** projected along the crystallographic *a*-axis. The C_{60} molecules are drawn in spacefill style and the hydrogen atoms are omitted for clarity.

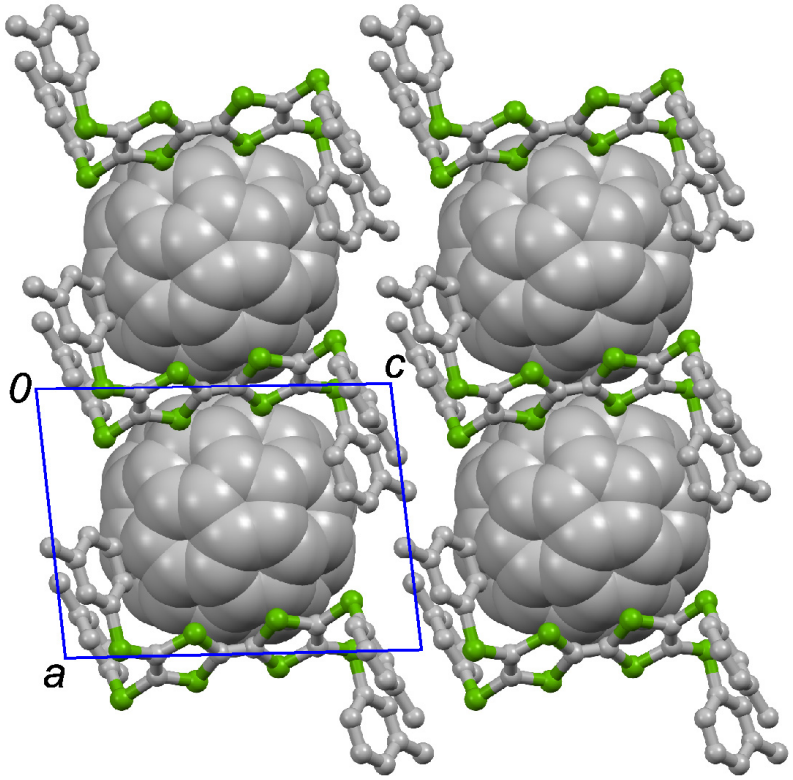

Fig. S8 Crystal structure of **TTF2•C_{60}** projected along the crystallographic *b*-axis. The C_{60} molecules are drawn in spacefill style and the hydrogen atoms are omitted for clarity.

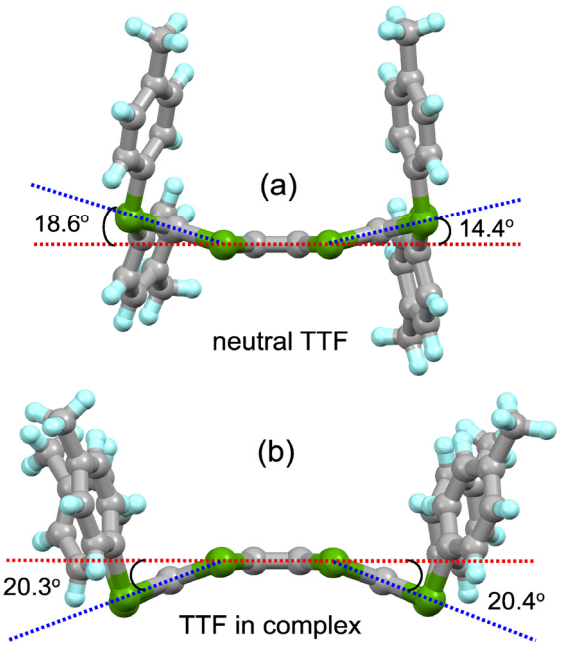

Fig. S9 Molecular geometry of **TTF3** in the pure neutral crystal and in the complex **TTF3•(C_{70})$_2$•(PhCl)$_2$**. The figure shows the molecular geometry of TTF molecule ***A*** in complex, and that of TTF molecule ***B*** is almost identical to this depiction. The red and blue dashed lines represent the mean planes of central C_2S_4 and terminal C_2S_2 framework of TTF skeleton, respectively.

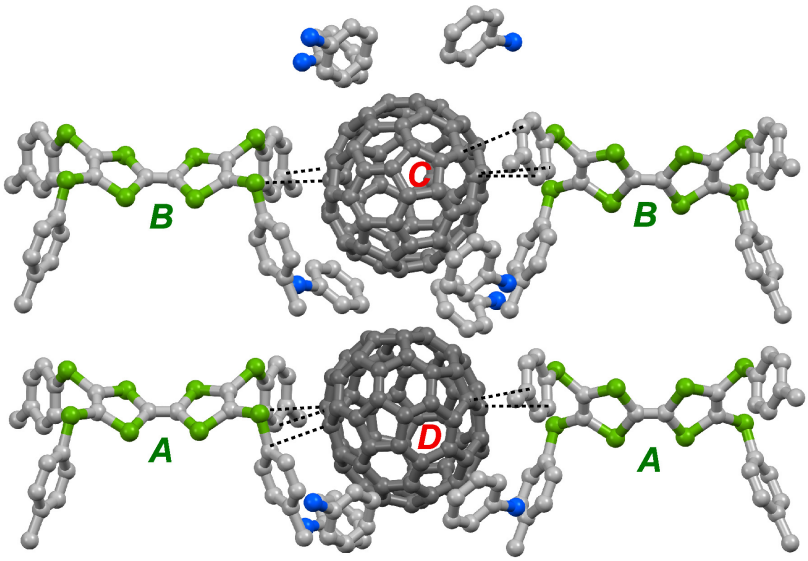

Fig. S10 Encapsulation of **C_{70}** molecules (***C*** and ***D***) by **TTF3** molecules (***A*** and ***B***) and solvent molecule **PhCl** in **TTF3•(C_{70})$_2$•(PhCl)$_2$**. The black dashed lines indicate the intermolecular C–C atomic short contacts between the TTF3 and C_{70}. The atomic close contacts were also observed between the PhCl molecules and C_{70} molecules. For molecule ***C***, short contacts with PhCl molecules ***J*** and ***K*** are observed: two C–Cl contacts (3.39 and 3.44 Å) and two C–C contacts (3.29 and 3.35 Å). For molecule ***D***, short contacts between it and PhCl molecules ***L*** and ***M*** are observed: one C–Cl contact of 3.40 Å and two C–C contacts (3.29 and 3.37 Å).

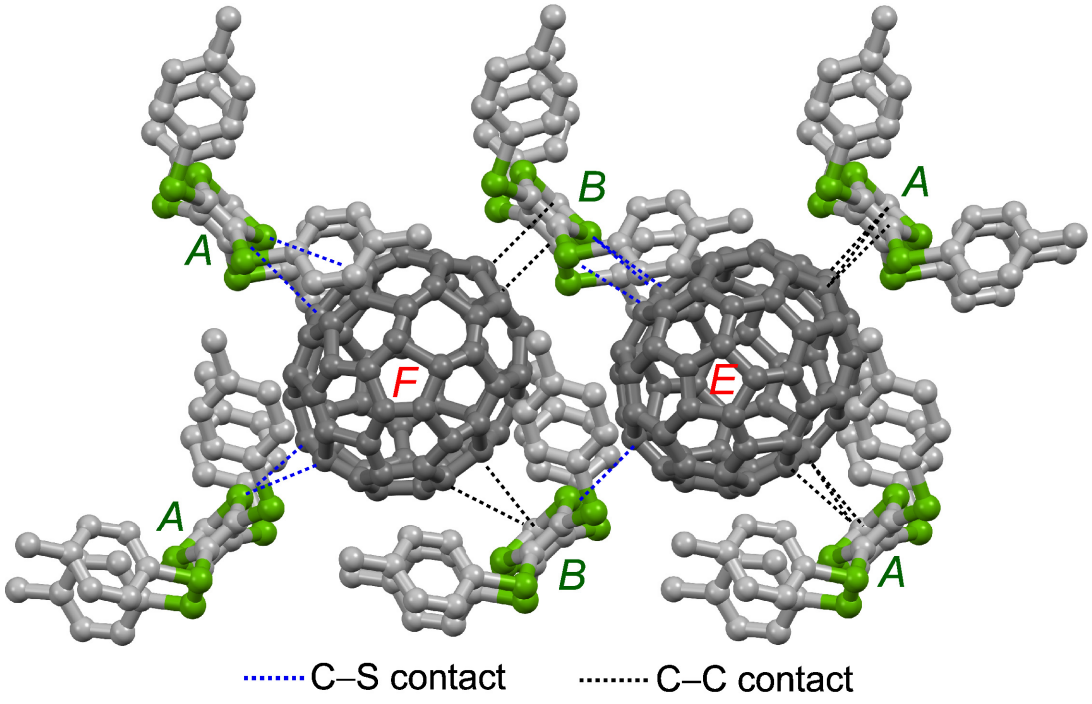

Fig. S11 Encapsulation of C_{70} molecules (***E*** and ***F***) by **TTF3** molecules (***A*** and ***B***) in complex **TTF3•$(C_{70})_2$•$(PhCl)_2$**. The black and blue dashed lines indicate the intermolecular C–C and C–S atomic short contacts respectively.

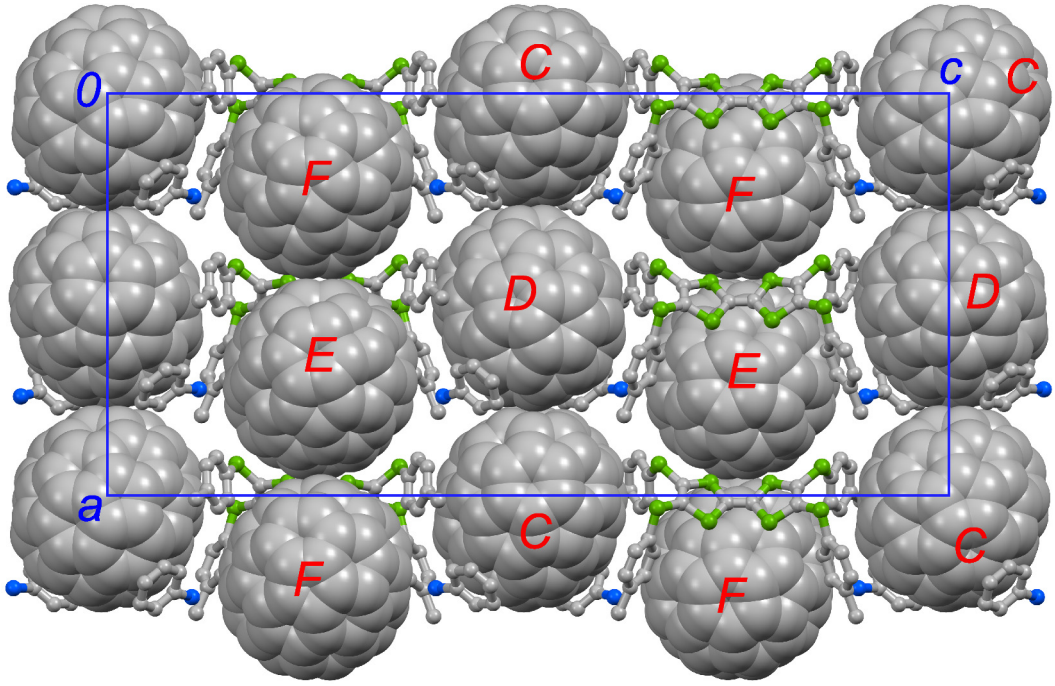

Fig. S12 Crystal structure of **TTF3•$(C_{70})_2$•$(PhCl)_2$** projected along the crystallographic *b*-axis at y = 0.5. The C_{70} molecules (***C***, ***D***, ***E***, and ***F***) are drawn in the space-filled mode.

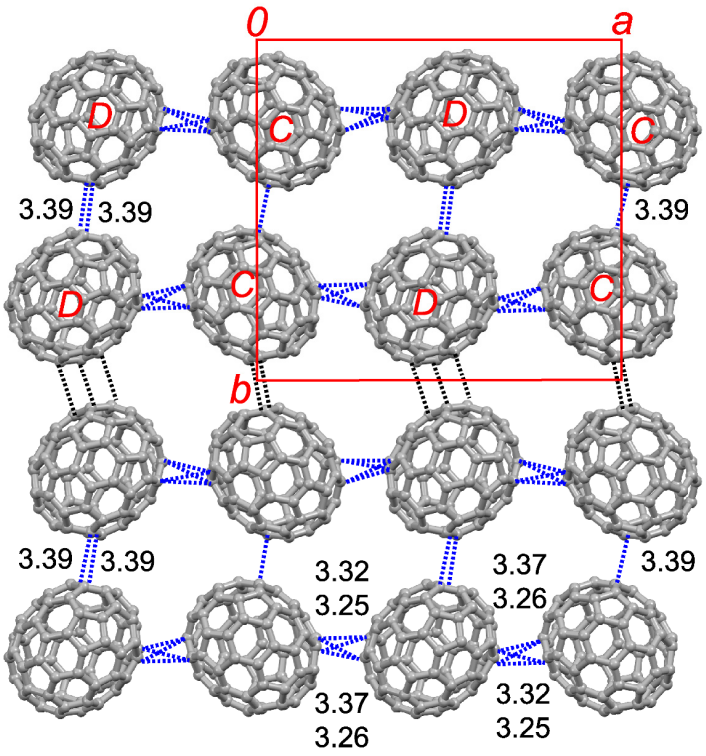

Fig. S13 Arrangement of C_{70} molecules in *ab*-plane at z = 0 in complex **TTF3•$(C_{70})_2$•$(PhCl)_2$**. The blue dashed lines with numbers indicate the intermolecular C–C close contacts, and the black dashed lines indicate the pseudo C-C contacts, which are 3.42 Å.

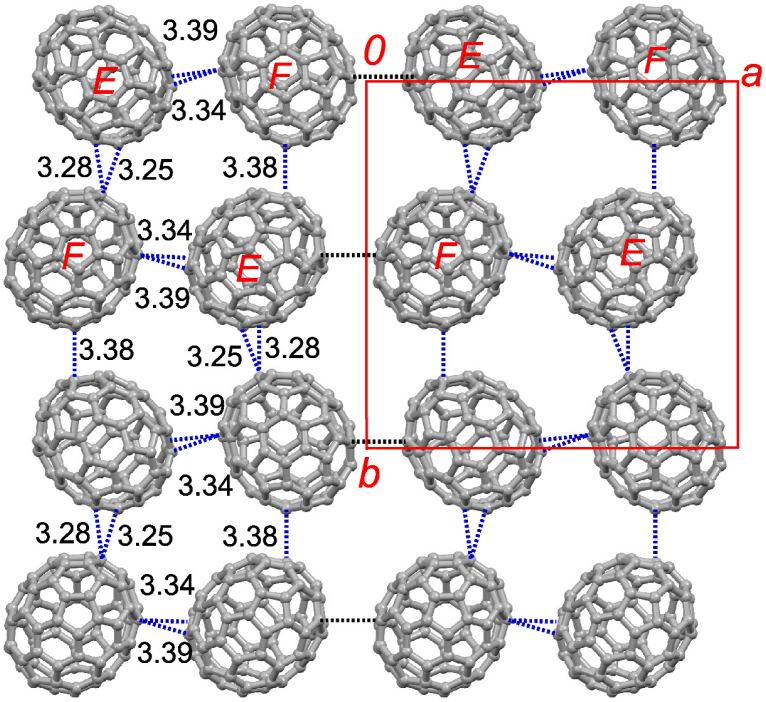

Fig. S14 Arrangement of C_{70} molecules in *ab*-plane at z = 0.5 in complex **TTF3•$(C_{70})_2$•$(PhCl)_2$**. The blue dashed lines with numbers indicate the intermolecular close C-C contacts, and the black dashed lines indicate the pseudo C-C contacts, which are 3.42 Å.

Optical absorption spectra

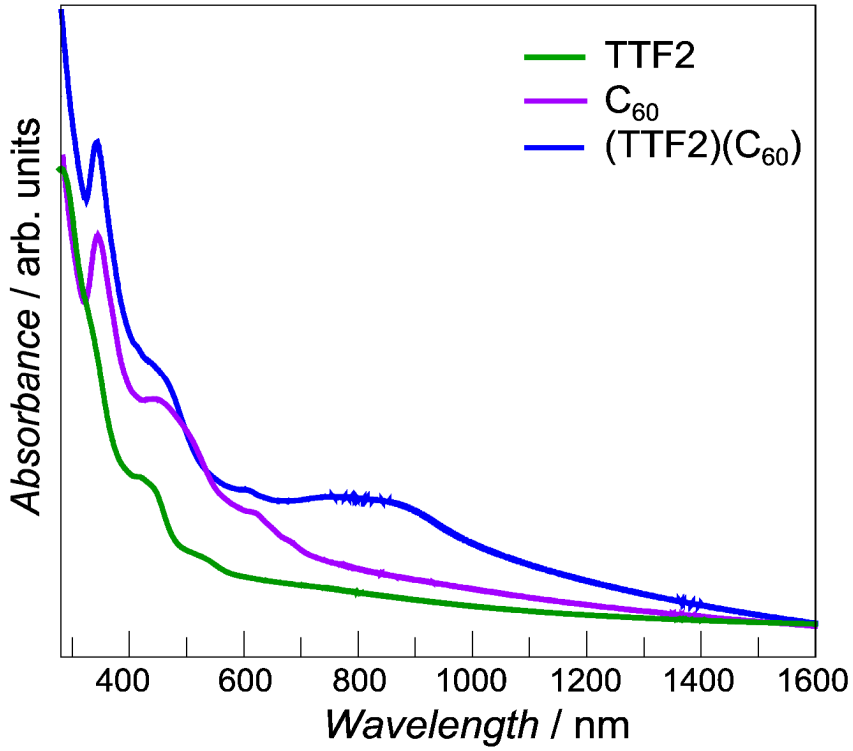

Fig. S15 Solid state absorption spectra of **TTF2•C_{60}** along with those of **TTF2** and **C_{60}** for comparison. The spectra were measured on the dispersed samples in KBr pellet.

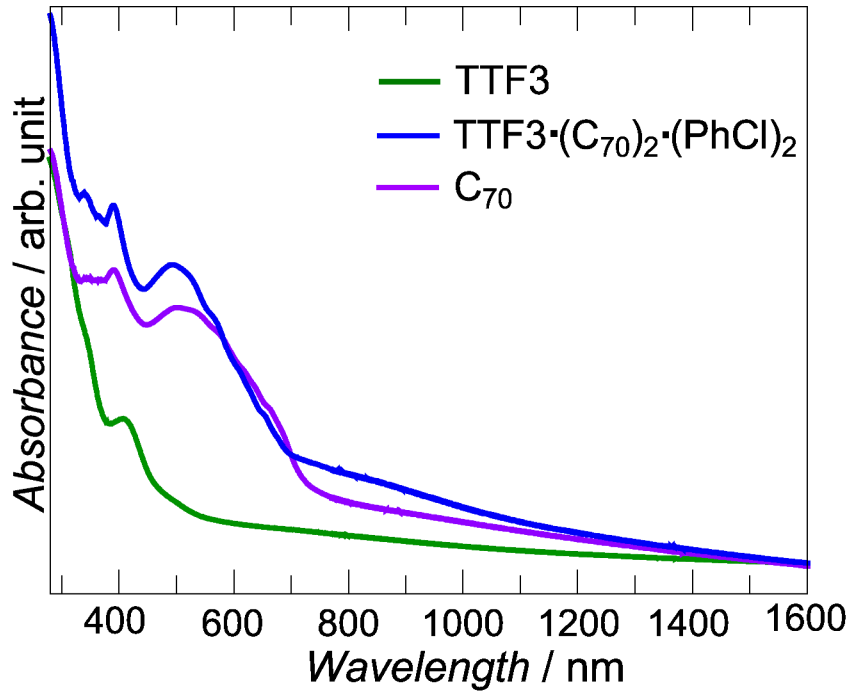

Fig. S16 Solid state absorption spectra of **TTF3•$(C_{70})_2$•$(PhCl)_2$** along with those of **TTF3** and **C_{70}** for comparison. The spectra were measured on the dispersed samples in KBr pellet.

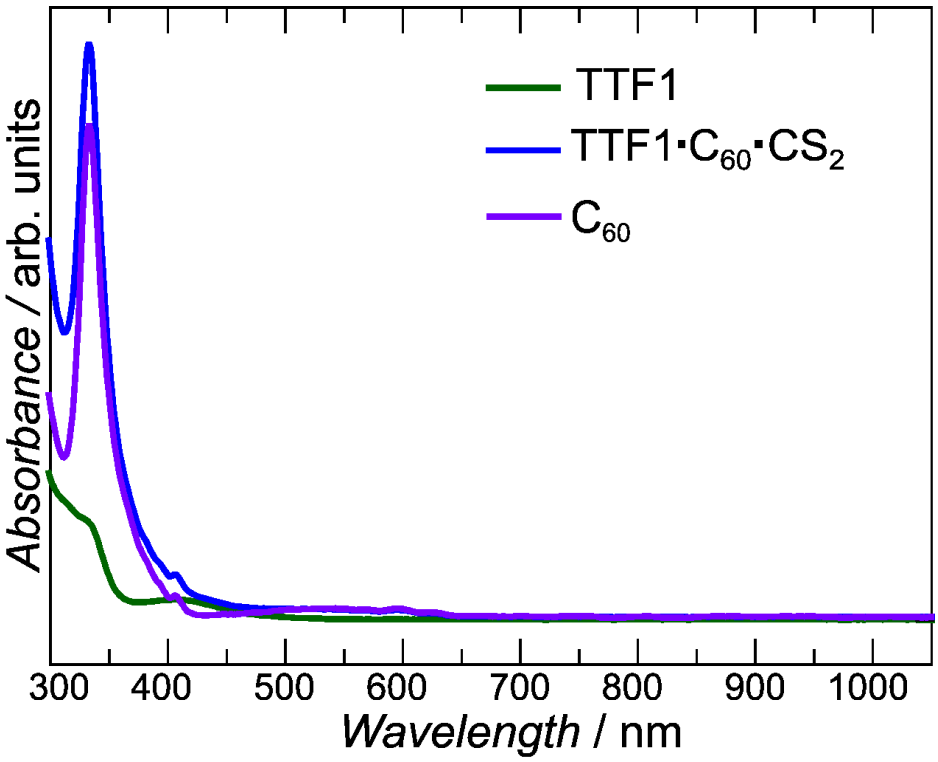

Fig. S17 UV-Vis absorption spectra of **TTF1•C_{60}•CS_2** in PhCl solution (C = 10^{-4} mol L^{-1}), along with those of **TTF1** and **C_{60}** for comparison.

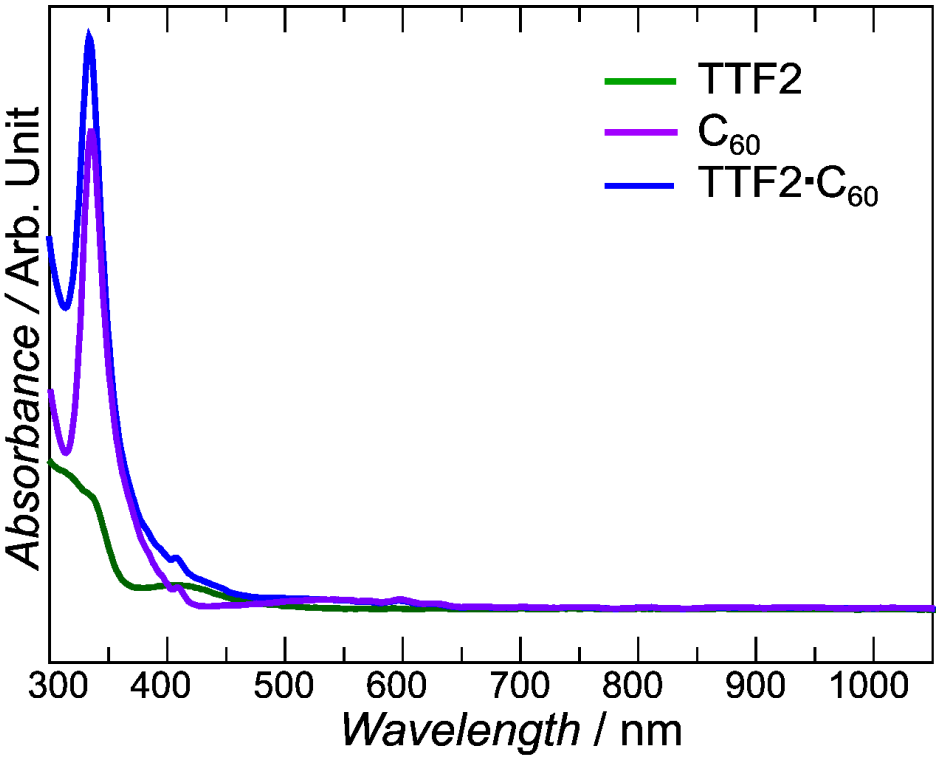

Fig. S18 UV-Vis absorption spectra of **TTF2•C_{60}** in PhCl solution (C = 10^{-4} mol L^{-1}), along with those of **TTF2** and **C_{60}** for comparison.

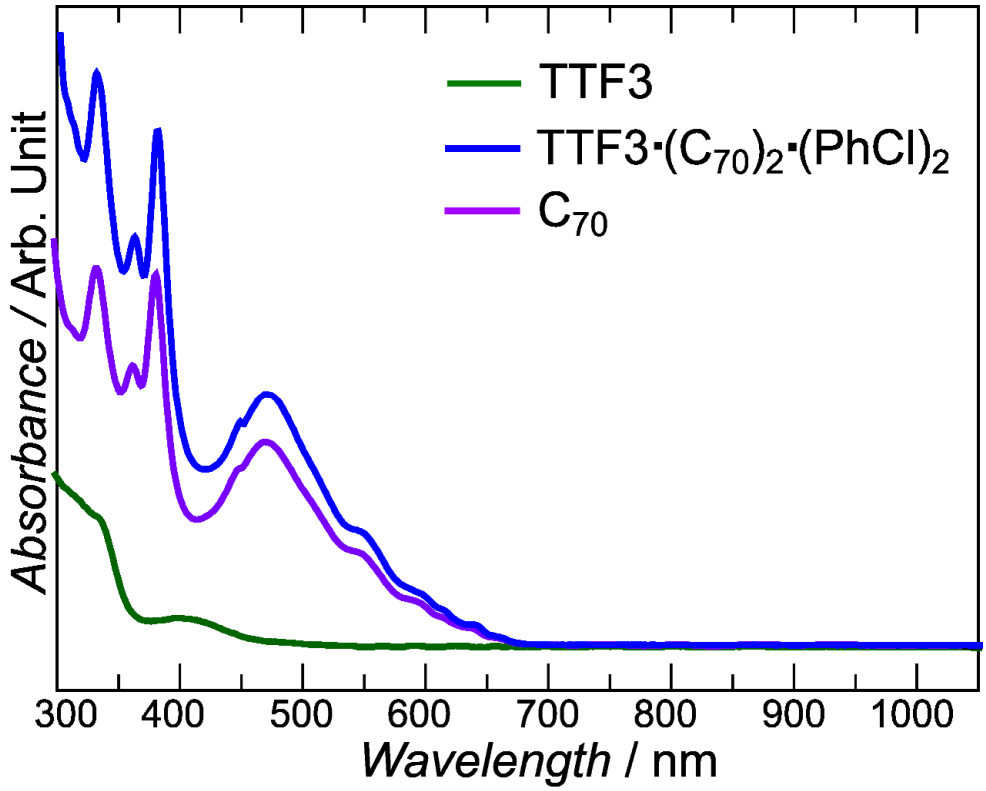

Fig. S19 UV-Vis absorption spectra of **TTF3•$(C_{70})_2$•$PhCl_2$** in PhCl solution (C = 10^{-4} mol L^{-1}), along with those of **TTF3** and **C_{70}** for comparison.

IR spectra

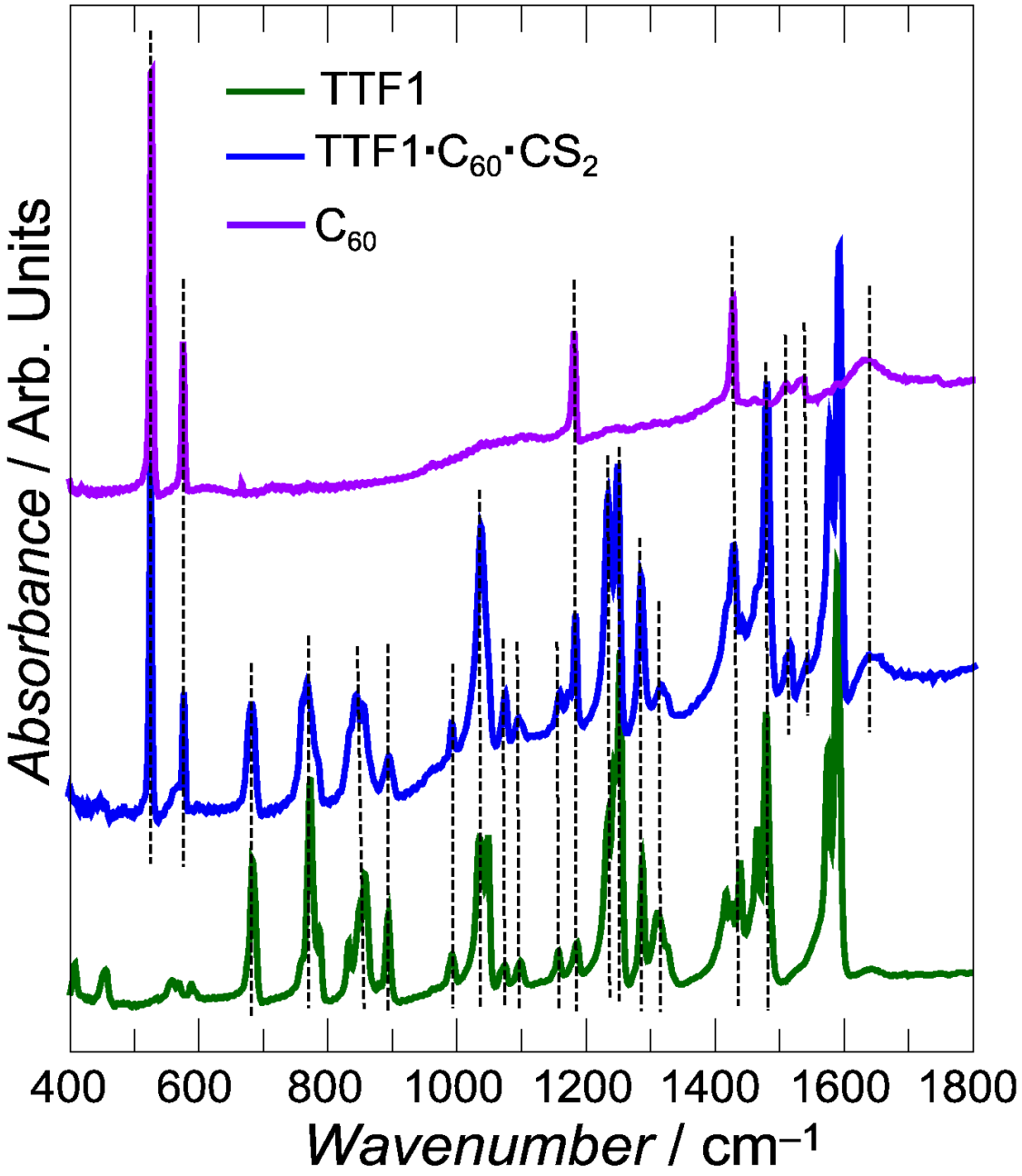

Fig. S20 IR spectra of **TTF1•C_{60}•CS_2** along with those of **TTF1** and **C_{60}** for comparison (in KBr). The black dashed lines are guides for the eye.

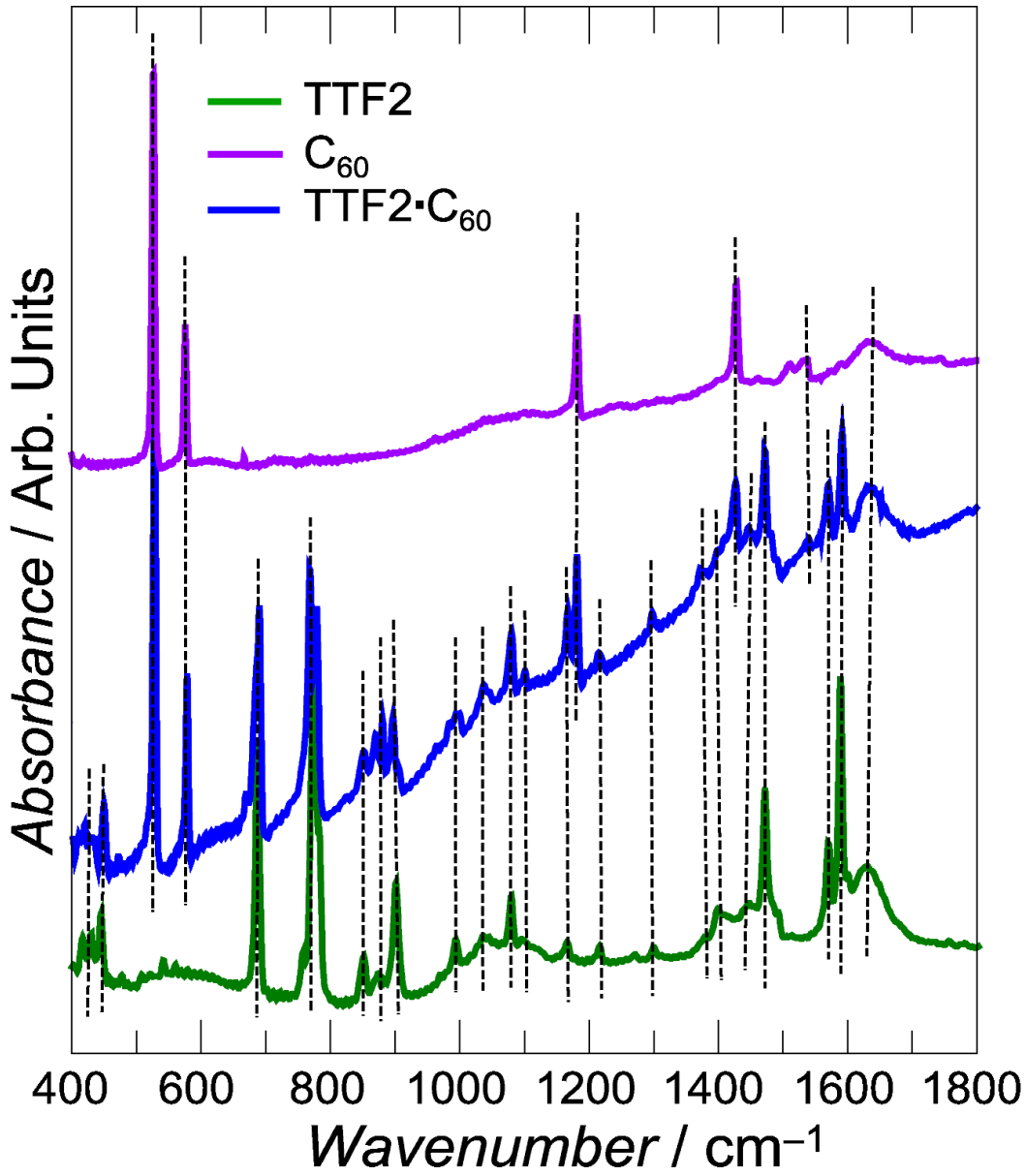

Fig. S21 IR spectra of **TTF2•C_{60}** along with those of **TTF2** and **C_{60}** for comparison (in KBr). The black dashed lines are guides for the eye.

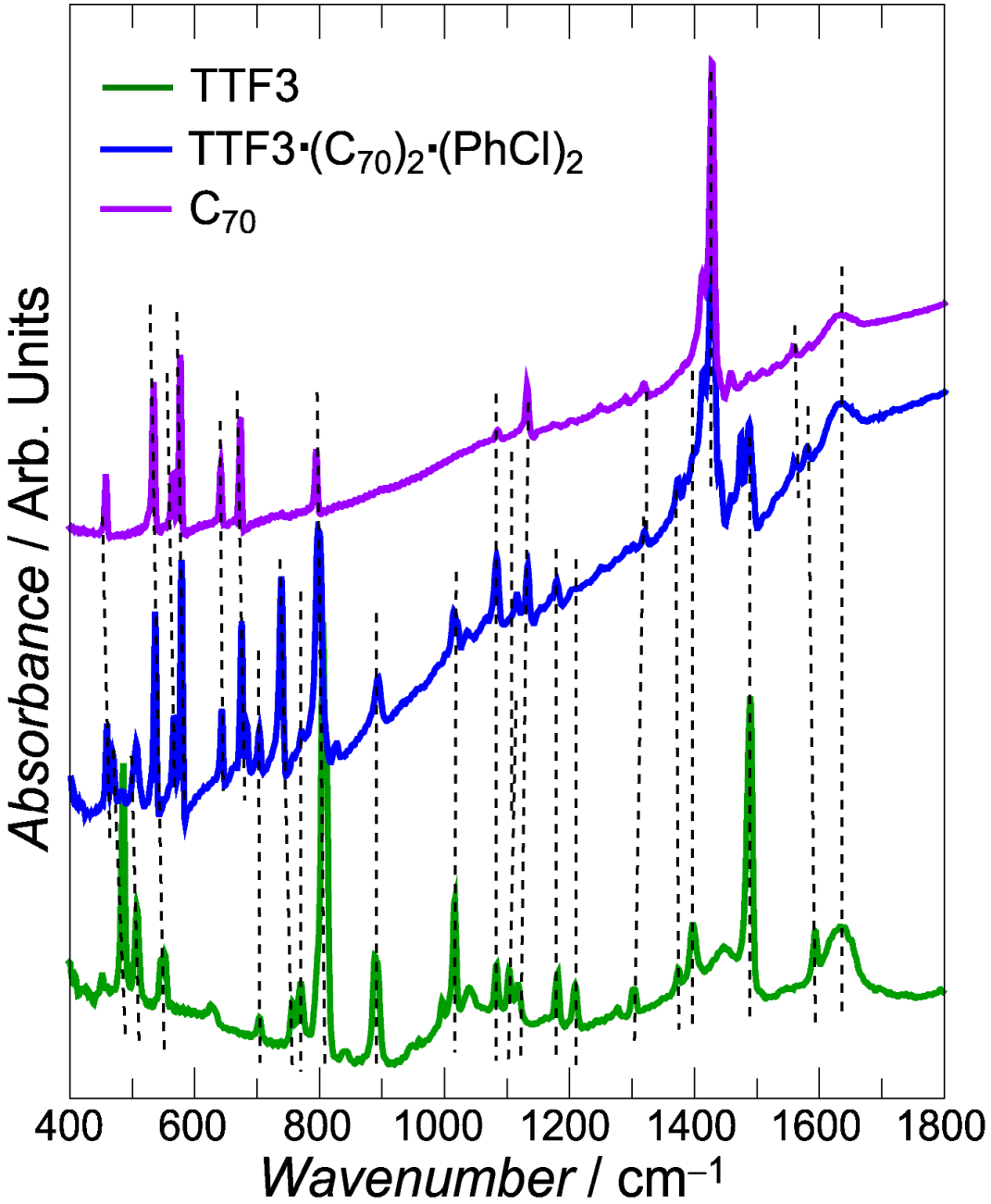

Fig. S22 IR spectra of **TTF3•C_{70})$_2$•(PhCl)$_2$** along with those of **TTF3** and **C_{70}** for comparison (in KBr). The black dashed lines are guides for the eye.

Theoretical calculations

The electronic structures of ground (S_0) and excited states (S_n, $n \geq 1$) were investigated by density functional theory (DFT) and time-dependent DFT (TD-DFT) methods based on X-ray structure without carbon disulfide and chlorobenzene molecules, respectively (Fig. S23 and Table S3). The energy diagrams of frontier orbitals for **TTF1•C_{60}** and **TTF3•$(C_{70})_2$** clusters are shown in Figs. S24–S26 and S27–S29, and the excitation properties are summarized in Table S4 and S5, respectively.

As for **TTF1•C_{60}** cluster, the three functionals afforded similar frontier orbitals although the orbital energies depend on the type of functional. The highest occupied molecular orbital (HOMO) is localized on the TTF moiety, whereas the lowest unoccupied molecular orbital (LUMO), (LU+1)MO, and (LU+2)MO are located on C_{60} molecule, which are quasi-triply-degenerated. Considering the calculated charges (Table S4), TTF1 and C_{60} molecules are nearly neutral at the S_0 state, which supports the result of infrared spectroscopy.

All three functionals showed that the $S_0 \rightarrow S_1$ transitions are characterized mainly as HOMO → LUMO excitation with very small oscillator strengths although the calculated excitation energies are significantly dependent on the type of functional, which were underestimated with B3LYP and overestimated with long-range corrected functionals, CAM-B3LYP and ωB97X-D. The $S_0 \rightarrow S_2$ transitions have larger oscillator strengths than the $S_0 \rightarrow S_1$ transition, which is described mainly as HOMO → (LU+1)MO excitation with B3LYP, and HOMO → (LU+1)MO and (LU+2)MO excitations with CAM-B3LYP and ωB97X-D. As for the $S_0 \rightarrow S_3$ transitions, they are regarded mainly as HOMO → (LU+2)MO excitation with B3LYP, HOMO → (LU+2)MO and (LU+1)MO excitations with CAM-B3LYP, and (HO−1)MO → LUMO with negligible oscillator strength by ωB97X-D. Therefore, the $S_0 \rightarrow S_2$ and $S_0 \rightarrow S_3$ transitions with B3LYP, and the $S_0 \rightarrow S_2$ transition with CAM-B3LYP and ωB97X-D are dominant on the new band observed in TTF1·C_{60}·CS_2 complex. In other words, all three functionals conclude that the HOMO → (LU+1)MO and (LU+2)MO excitations are dominant on the new band although they afforded the slightly different results. Comparing the charge distribution at the S_2 and S_3 states with B3LYP and the S_2 states with CAM-B3LYP and ωB97X-D to the corresponding S_0 states, these transitions are described as electronic transition from the neutral ground state to the charge-separated excited state.

As for **TTF3•$(C_{70})_2$** cluster, the three functionals also afforded similar frontier orbitals with the orbital energies depending on the type of functional like the case of TTF1•C_{60} cluster. The highest

occupied molecular orbital (HOMO) is localized on the TTF moiety, whereas the LUMO, (LU+1)MO, and (LU+2)MO are located on C_{70}(L) molecule, and the (LU+3)MO, (LU+4)MO, and (LU+5)MO are located on C_{70}(R) molecule, which are quasi-triply-degenerated. Considering the calculated charges (Table S5), TTF3 and C_{70} molecules are nearly neutral at the S_0 state, which supports the result of infrared spectroscopy.

In the case of B3LYP functional, the low-lying transitions of $S_0 \rightarrow S_1$, S_2, S_3, S_4, S_5, and S_6 are characterized as HOMO → LUMO, (LU+1)MO, and (LU+2)MO excitations, and HOMO → (LU+3)MO, (LU+4)MO, and (LU+5)MO excitations. Also considering the calculated charges (Table S5), all these transitions are regarded as electronic transition from the neutral ground state to the charge-separated excited state.

However, the long-range corrected CAM-B3LYP functional predicted the slightly different result from the B3LYP functional. The lowest $S_0 \rightarrow S_1$ transition is characterized as HOMO → (LU+2)MO and (LU+1)MO excitations, which is the electronic transition from the neutral ground state to the charge-separated excited state. The second and third lowest transitions of $S_0 \rightarrow S_2$ and S_3 are regarded as the local excitations of C_{70}(R) and C_{70}(L) molecules, respectively. The fourth lowest $S_0 \rightarrow S_4$ transition is characterized mainly as HOMO → LUMO and (LU+2)MO excitations, which is not the local, but the charge transfer excitation.

As for another long-range corrected ωB97X-D functional, the lowest and second lowest transitions of $S_0 \rightarrow S_1$ and S_2 are not described as the charge transfer, but the local excitation on C_{70}(L) and C_{70}(R) molecules, respectively. The third lowest $S_0 \rightarrow S_3$ transition is regarded mainly as HOMO → (LU+2)MO and (LU+1)MO excitations, characteristic of the charge-separated excited state.

Although B3LYP, CAM-B3LYP, and ωB97X-D afforded the slightly different results probably due to the mixing ratio of HF exchange, all three functional predicts the low-lying transition from neutral ground state to charge-separated excited state. Therefore, it is concluded that the new band observed in **TTF_3•$(C_{70})_2$•$(PhCl)_2$** complex contains the charge transfer character from TTF3 to C_{70} molecule.

Computational details

Density functional theory (DFT) and time-dependent DFT (TD-DFT) calculations by B3LYP,[1] CAM-B3LYP,[2] and ωB97X-D[3] were carried out based on X-ray structure. The solvent molecules CS_2 and PhCl were not included in the present calculation. B3LYP is a widely used hybrid

functional which contains 20% Hartree–Fock (HF) exchange. However, B3LYP has a tendency to underestimate the charge transfer (CT) excitation energies.[2] CAM-B3LYP and ωB97X-D are long-range corrected functionals which are considered appropriate for CT excitations. CAM-B3LYP includes 19% HF exchange at short-range and 65% HF exchange at long-range, whereas ωB97X-D includes 22% HF exchange at short-range and 100% HF exchange at long-range and also corrected by empirical dispersion.[4] The double-ζ basis set with polarization functions of d-type on heavy atoms and p-type on hydrogen (6-31G(d,p)[5]) was used. All of the computations were performed with the Gaussian 09 program package.[6] Natural population analyses were carried out with the NBO program.[7]

References

[1] K. Ragavachari, *Theor. Chem. Acc*., 2000, **103**, 361 and references cited therein.

[2] a) T. Yanai, D. Tew and N. Handy, *Chem. Phys. Lett.,* 2004, **393**, 51; b) M. J. G. Peach, P. Benfield, T. Helgaker and D. J. Tozer, *J. Chem. Phys.,* 2008, **128**, 044118.

[3] J. -Da. Chai and M. Head-Gordon, *Phys. Chem. Chem. Phys.,* 2008, **10**, 6615.

[4] S. Grimme, *J. Comput. Chem.,* 2008, **27**, 1787.

[5] a) W. J. Hehre, R. Ditchfield and J. A. Pople, *J. Chem. Phys.,* 1972, **56**, 2257; b) P. C. Hariharan and J. A. Pople, *Mol. Phys.,* 1974, **27**, 209; c) P. C. Hariharan and J. A. Pople, *Theo. Chim. Acta* 1973, **28**, 213; d) M. M. Francl, W. J. Pietro, W. J. Hehre, J. S. Binkley, M. S. Gordon, D. J. DeFrees and J. A. Pople, *J. Chem. Phys.,* 1982, **77**, 3654.

[6] Gaussian 09, Revision D.01, M. J. Frisch, G. W. Trucks, H. B. Schlegel, G. E. Scuseria, M. A. Robb, J. R. Cheeseman, G. Scalmani, V. Barone, B. Mennucci, G. A. Petersson, H. Nakatsuji, M. Caricato, X. Li, H. P. Hratchian, A. F. Izmaylov, J. Bloino, G. Zheng, J. L. Sonnenberg, M. Hada, M. Ehara, K. Toyota, R. Fukuda, J. Hasegawa, M. Ishida, T. Nakajima, Y. Honda, O. Kitao, H. Nakai, T. Vreven, J. A. Montgomery, Jr., J. E. Peralta, F. Ogliaro, M. Bearpark, J. J. Heyd, E. Brothers, K. N. Kudin, V. N. Staroverov, T. Keith, R. Kobayashi, J. Normand, K. Raghavachari, A. Rendell, J. C. Burant, S. S. Iyengar, J. Tomasi, M. Cossi, N. Rega, J. M. Millam, M. Klene, J. E. Knox, J. B. Cross, V. Bakken, C. Adamo, J. Jaramillo, R. Gomperts, R. E. Stratmann, O. Yazyev, A. J. Austin, R. Cammi, C. Pomelli, J. W. Ochterski, R. L. Martin, K. Morokuma, V. G. Zakrzewski, G. A. Voth, P. Salvador, J. J. Dannenberg, S. Dapprich, A. D. Daniels, O. Farkas, J. B. Foresman, J. V. Ortiz, J. Cioslowski and D. J. Fox, Gaussian, Inc., Wallingford CT, 2013.

[7] NBO Version 3.1, E. D. Glendening, A. E. Reed, J. E. Carpenter, and F. Weinhold.

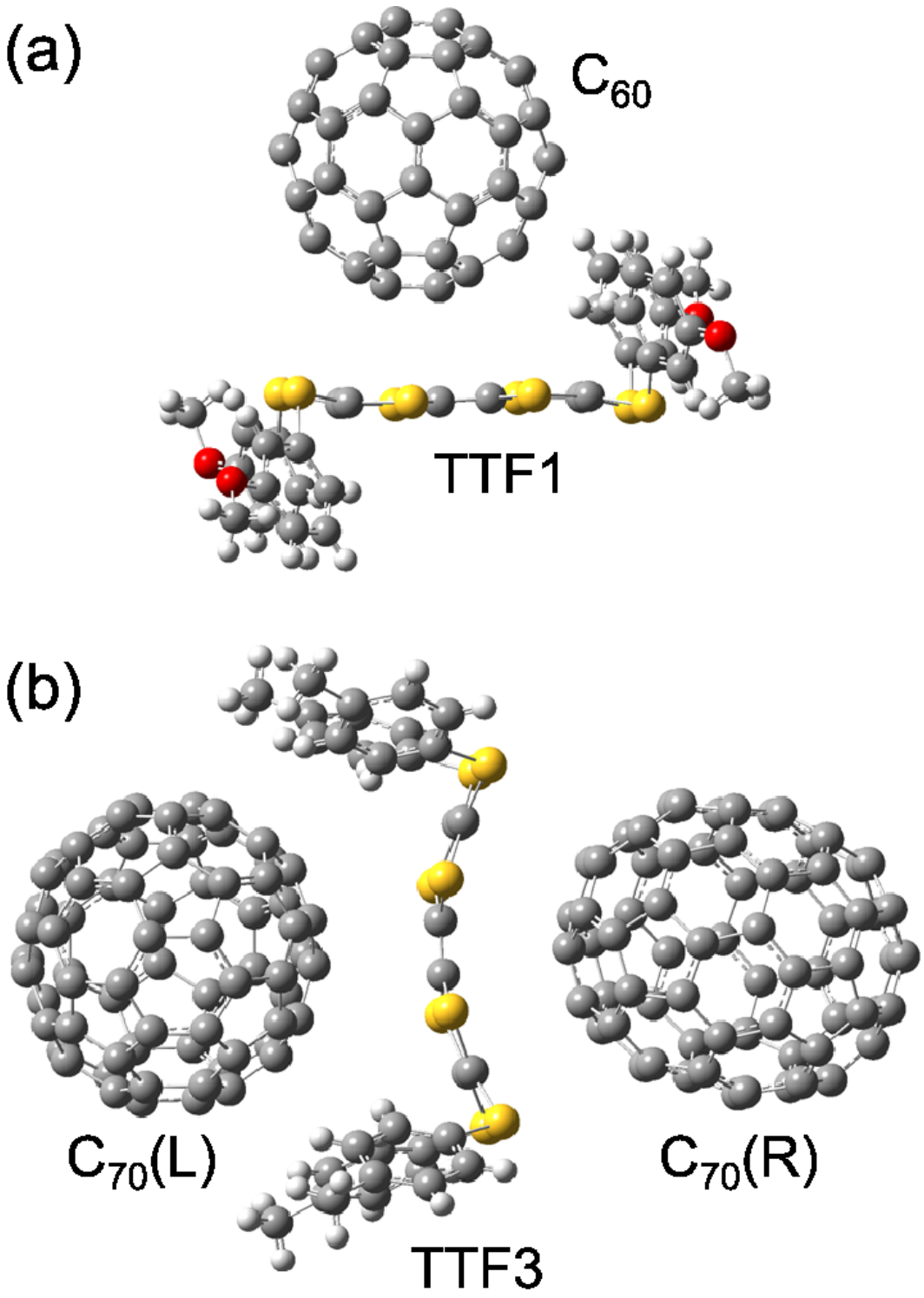

Fig. S23 Calculated geometries of (a) **TTF1•C_{60}** and (b) **TTF3•$(C_{70})_2$** clusters, in which TTF3 is molecule A, and C_{70}(L) and C_{70}(R) are molecules E.

Table S3. Total energies (E) and HOMO-LUMO gaps ($\Delta E_{\text{HOMO-LUMO}}$) for **TTF1•$C_{60}$** and **[$C_{70}$(E)-TTF3(A)-$C_{70}$(E)]** clusters calculated at the B3LYP, CAM-B3LYP, and ωB97X-D/6-31G(d,p) levels of theory.

Method	E / hartree	$\Delta E_{\text{HOMO-LUMO}}$ / eV
TTF1•C_{60}		
B3LYP/6-31G(d,p)	−7084.4158	1.569
CAM-B3LYP/6-31G(d,p)	−7082.2940	3.822
ωB97X-D/6-31G(d,p)	−7083.0679	4.863
[C_{70}(E)-TTF3(A)- C_{70}(E)]		
B3LYP/6-31G(d,p)	−9832.0148	1.575
CAM-B3LYP/6-31G(d,p)	−9828.3286	3.710
ωB97X-D/6-31G(d,p)	−9829.8309	4.737

Table S4. Excitation energies (ΔE), oscillator strengths (f), assignments, and charges[a] of TTF1 molecule by Mulliken and natural population analyses (NPA) in the ground (S_0) and low-lying excited (S_1, S_2, and S_3) states for **TTF1•C_{60}** cluster calculated at the TD-(B3LYP, CAM-B3LYP, and ωB97X-D)/6-31G(d,p) levels of theory.

State	ΔE / eV	f	Assignment	Mulliken	NPA
B3LYP					
S_0				−0.032	+0.039
S_1	1.132	0.0004	HO → LU (99%)	+0.831	+0.957
S_2	1.232	0.0034	HO → LU+1 (96%)	+0.824	+0.951
			HO → LU+2 (3%)		
S_3	1.290	0.0040	HO → LU+2 (96%)	+0.826	+0.950
			HO → LU+1 (3%)		
CAM-B3LYP					
S_0				−0.041	+0.030
S_1	2.303	0.0008	HO → LU (88%)	+0.784	+0.907
			HO → LU+3 (4%)		
S_2	2.409	0.0066	HO → LU+1 (57%)	+0.763	+0.886
			HO → LU+2 (32%)		
			HO → LU+5 (4%)		
S_3	2.564	0.0003	HO → LU+2 (53%)	+0.714	+0.830
			HO → LU+1 (33%)		
			HO−1 → LU (3%)		
ωB97X-D					
S_0				−0.034	+0.030
S_1	2.496	0.0010	HO → LU (78%)	+0.725	+0.837
			HO → LU+3 (6%)		
			HO → LU+4 (3%)		
			HO−5 → LU (3%)		
			HO−4 → LU (3%)		
S_2	2.602	0.0067	HO → LU+1 (42%)	+0.657	+0.766
			HO → LU+2 (32%)		
			HO → LU+5 (6%)		
			HO−5 → LU+2 (2%)		
S_3	2.656	0.0003	HO−1 → LU (44%)	+0.000	+0.068
			HO−2 → LU (18%)		
			HO−3 → LU (13%)		
			HO−4 → LU (8%)		
			HO−6 → LU (2%)		

[a] C_{60} molecule has the charge equal in magnitude and opposite in sign.

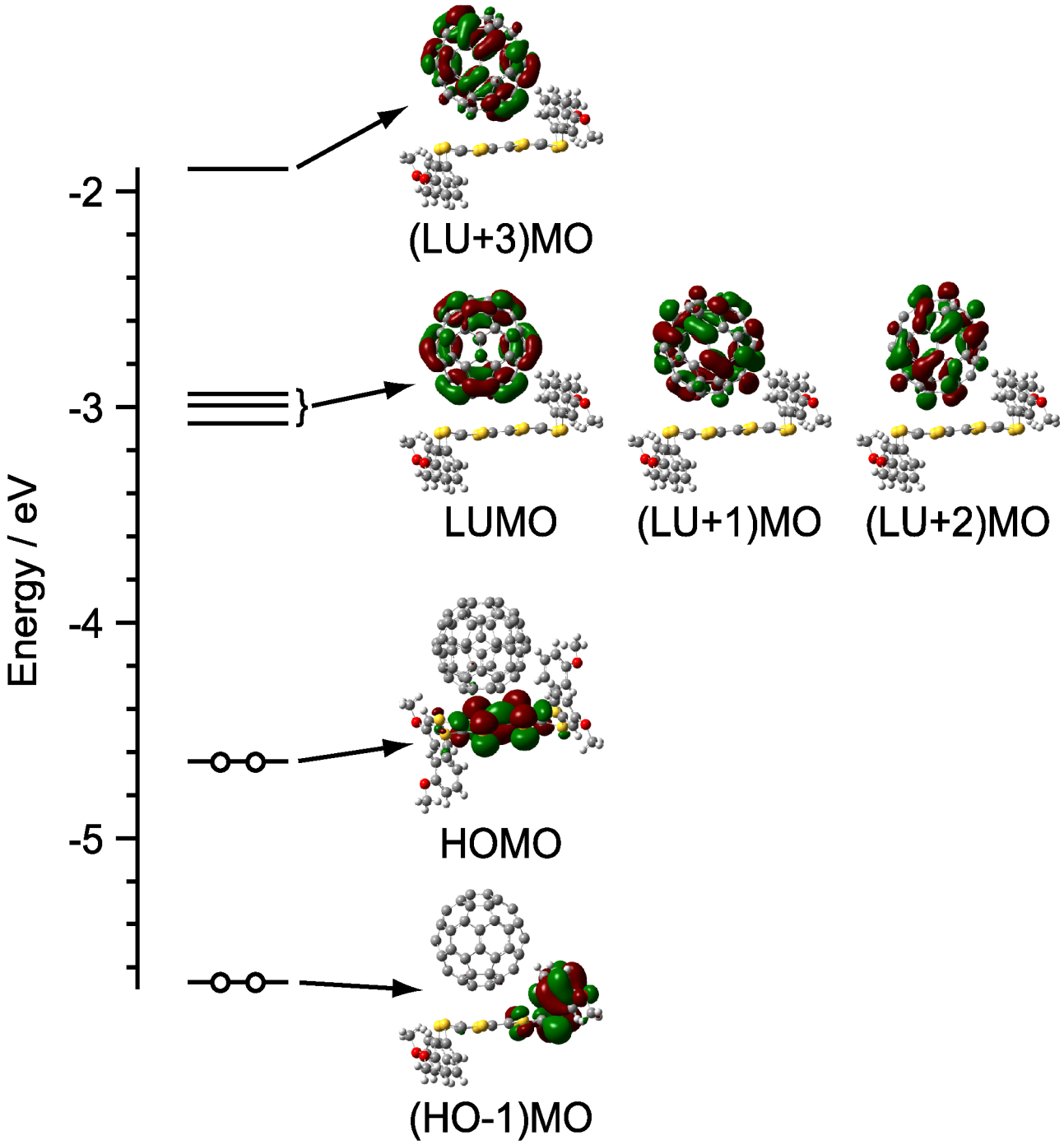

Fig. S24 Energy diagram of frontier Kohn-Sham orbitals for **TTF1•C_{60}** cluster calculated at the B3LYP/6-31G(d,p) level of theory.

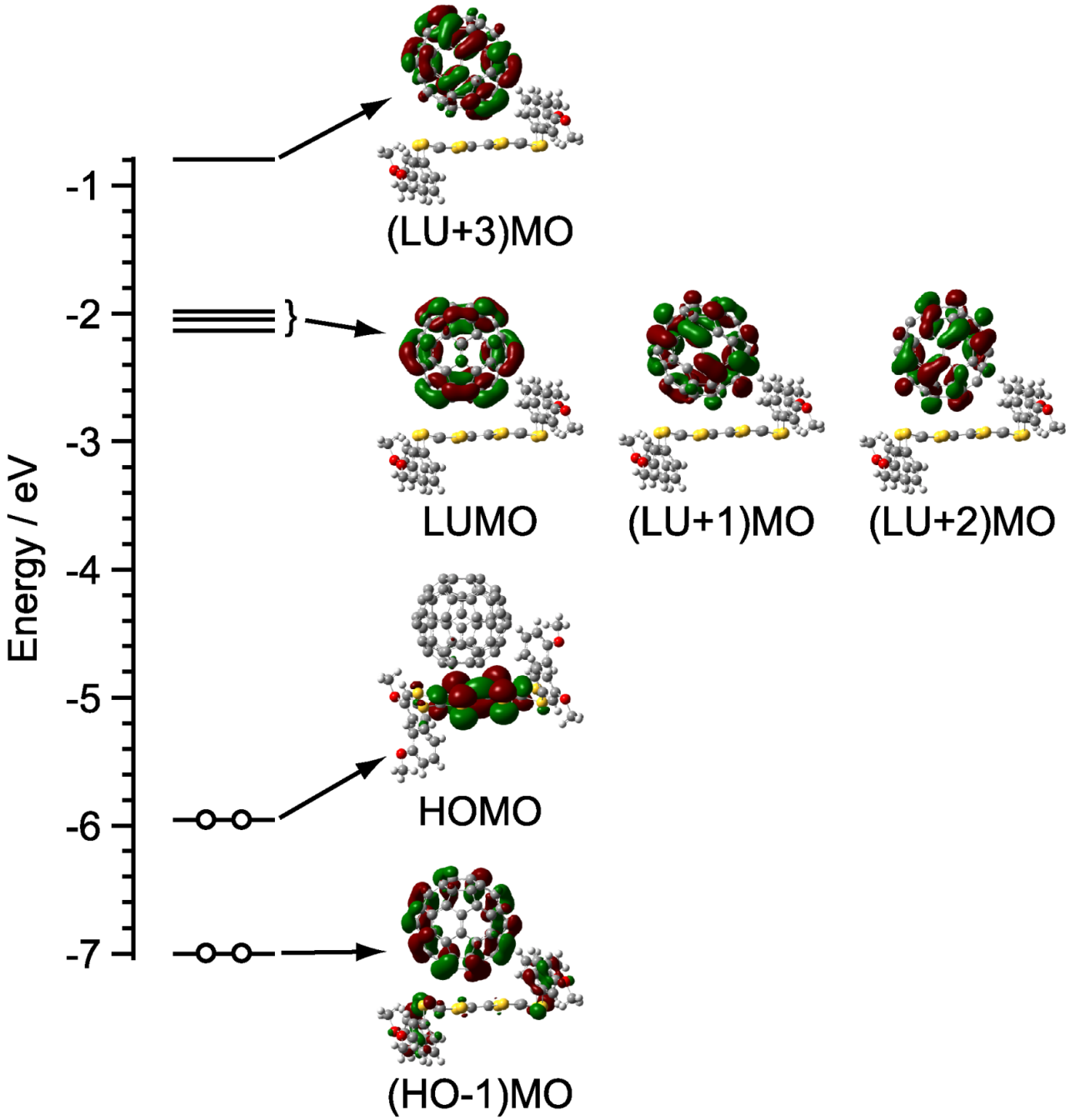

Fig. S25 Energy diagram of frontier Kohn-Sham orbitals for **TTF1•C_{60}** cluster calculated at the CAM-B3LYP/6-31G(d,p) level of theory.

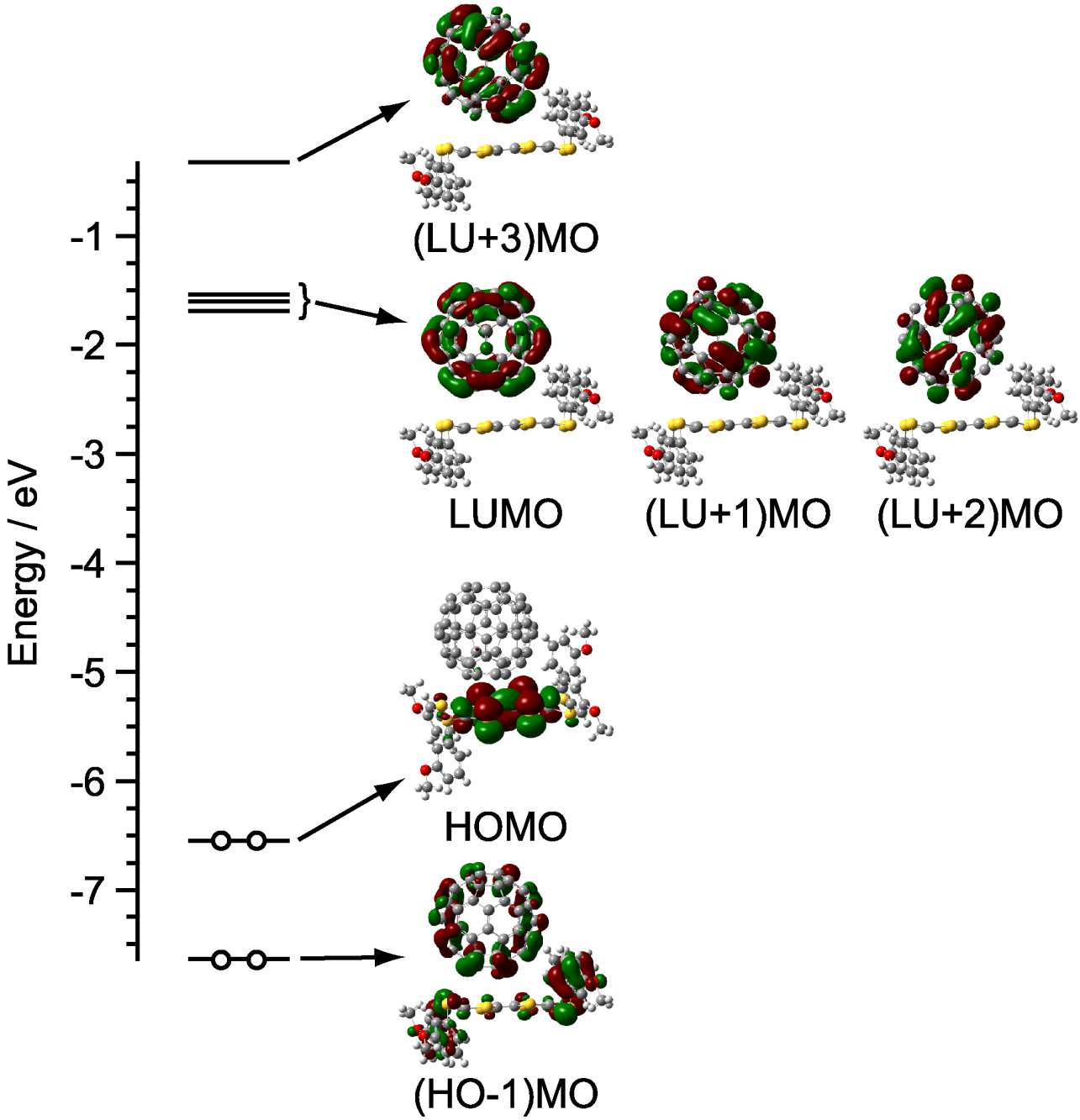

Fig. S26 Energy diagram of frontier Kohn-Sham orbitals for **TTF1•C_{60}** cluster calculated at the ωB97X-D/6-31G(d,p) level of theory.

Table S5. Excitation energies (ΔE), oscillator strengths (f), assignments, and charges[a] of TTF3, C_{70}(L), and C_{70}(R) molecules by Mulliken and natural population analyses (NPA) in the ground (S_0) and low-lying excited (S_1, S_2, S_3, S_4, S_5, and S_6) states for **TTF3·(C_{70})$_2$** cluster calculated at the TD-(B3LYP, CAM-B3LYP, and ωB97X-D)/6-31G(d,p) levels of theory.

				TTF3 **C_{70}(L)/C_{70}(R)**	
State	ΔE / eV	f	Assignment	Mulliken	NPA
B3LYP					
S_0				−0.053 +0.040/+0.013	+0.065 −0.025/−0.040
S_1	1.188	0.0086	HO → LU (91%) HO → LU+2 (5%) HO → LU+1 (4%)	+0.779 −0.829/+0.050	+0.955 −0.941/−0.015
S_2	1.239	0.0009	HO → LU+2 (95%) HO → LU (5%)	+0.788 −0.837/+0.049	+0.967 −0.951/−0.015
S_3	1.327	0.0021	HO → LU+1 (96%) HO → LU (4%)	+0.789 −0.840/+0.052	+0.964 −0.951/−0.014
S_4	1.482	0.0085	HO → LU+3 (95%) HO → LU+5 (3%)	+0.786 +0.073/−0.859	+0.962 −0.000/−0.961
S_5	1.573	0.0072	HO → LU+4 (89%) HO → LU+5 (10%)	+0.789 +0.074/−0.863	+0.964 +0.000/−0.965
S_6	1.634	0.0000	HO → LU+5 (86%) HO → LU+4 (10%) HO → LU+3 (3%)	+0.792 +0.075/−0.867	+0.965 +0.001/−0.966
CAM-B3LYP					
S_0				−0.068 +0.048/+0.021	+0.049 −0.017/−0.032
S_1	2.215	0.0099	HO → LU+2 (54%) HO → LU+1 (21%) HO → LU (9%) HO−4 → LU+3 (5%) HO−5 → LU (4%)	+0.624 −0.666/+0.042	+0.790 −0.771/−0.020
S_2	2.295	0.0009	HO−1 → LU+4 (40%) HO−2 → LU+3 (33%) HO−3 → LU+5 (11%) HO−2 → LU+4 (6%) HO−1 → LU+3 (3%) HO−1 → LU+5 (2%)	−0.065 +0.048/+0.018	+0.052 −0.017/−0.035

S_3	2.305	0.0009	HO−5 → LU (29%) HO−4 → LU+1 (27%) HO → LU+2 (16%) HO−5 → LU+1 (6%) HO−7 → LU+2 (5%) HO−4 → LU (5%) HO−4 → LU+2 (3%)	+0.103 −0.129/+0.026	+0.232 −0.203/−0.029
S_4	2.414	0.0079	HO → LU (71%) HO → LU+2 (13%) HO−4 → LU (4%) HO → LU+1 (2%)	+0.657 −0.701/+0.045	+0.822 −0.804/−0.018
S_5	2.507	0.0148	HO → LU+3 (43%) HO−1 → LU+3 (22%) HO → LU+5 (8%) HO−1 → LU+4 (7%) HO → LU+10 (4%) HO−1 → LU+5 (3%)	+0.346 +0.059/−0.404	+0.490 −0.010/−0.481
S_6	2.536	0.0095	HO−4 → LU (25%) HO−4 → LU+1 (25%) HO−5 → LU (11%) HO → LU+1 (10%) HO−4 → LU+2 (5%) HO → LU+2 (3%) HO−5 → LU+2 (2%)	+0.026 −0.051/+0.025	+0.148 −0.118/−0.030
***ω*B97X-D**					
S_0				−0.058 +0.040/+0.019	+0.049 −0.017/−0.032
S_1	2.294	0.0038	HO−4 → LU+1 (35%) HO−5 → LU (28%) HO−7 → LU+2 (8%) HO → LU+2 (6%) HO → LU+1 (5%) HO−4 → LU+2 (4%) HO−5 → LU+1 (3%)	+0.020 −0.041/+0.021	+0.133 −0.103/−0.031
S_2	2.309	0.0008	HO−1 → LU+4 (45%) HO−2 → LU+3 (32%) HO−3 → LU+5 (12%) HO−2 → LU+4 (3%)	−0.057 +0.040/+0.018	+0.050 −0.017/−0.033
S_3	2.414	0.0104	HO → LU+2 (59%) HO → LU+1 (20%) HO−5 → LU (6%) HO−4 → LU+1 (4%) HO → LU (3%)	+0.672 −0.711/+0.039	+0.830 −0.809/−0.021

S_4	2.589	0.0887	HO−4 → LU (19%) HO−5 → LU (14%) HO−4 → LU+1 (11%) HO−1 → LU+3 (10%) HO−2 → LU+3 (8%) HO−5 → LU+1 (6%) HO−1 → LU+4 (5%) HO−2 → LU+4 (2%)	−0.039 +0.020/+0.019	+0.070 −0.038/−0.032
S_5	2.591	0.0411	HO−2 → LU+3 (17%) HO−1 → LU+3 (16%) HO−1 → LU+4 (12%) HO−4 → LU (9%) HO−5 → LU (7%) HO−4 → LU+1 (5%) HO−2 → LU+4 (5%) HO−3 → LU+3 (4%) HO−5 → LU+1 (3%) HO−3 → LU+4 (2%)	−0.049 +0.032/+0.017	+0.060 −0.026/−0.034
S_6	2.614	0.0129	HO−1 → LU+3 (29%) HO−1 → LU+5 (10%) HO → LU+3 (8%) HO−2 → LU+3 (6%) HO−1 → LU+4 (6%) HO−3 → LU+4 (5%) HO → LU+5 (5%) HO−3 → LU+5 (4%) HO−3 → LU+3 (3%) HO−4 → LU (2%)	+0.030 +0.037/−0.066	+0.144 −0.022/−0.122

[a] The charge of TTF3 molecule is shown in the top line, and the charges of C_{70} molecules are shown in the bottom line, in the form of the charge of C_{70}(L)/the charge of C_{70}(R).

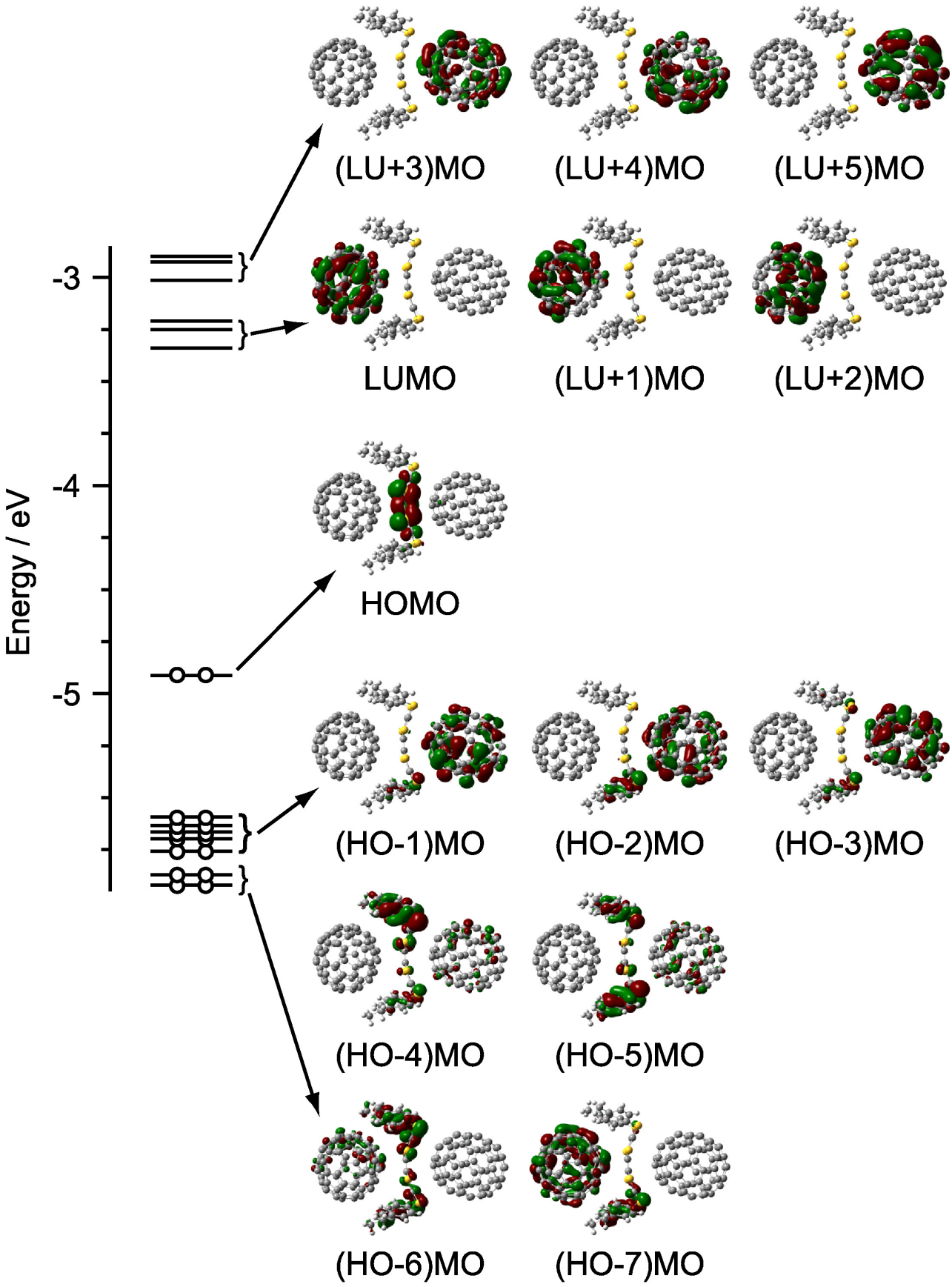

Fig. S27 Energy diagram of frontier Kohn-Sham orbitals for [C_{70}(L)-TTF3(A)-C_{70}(R)] cluster calculated at the B3LYP/6-31G(d,p) level of theory.

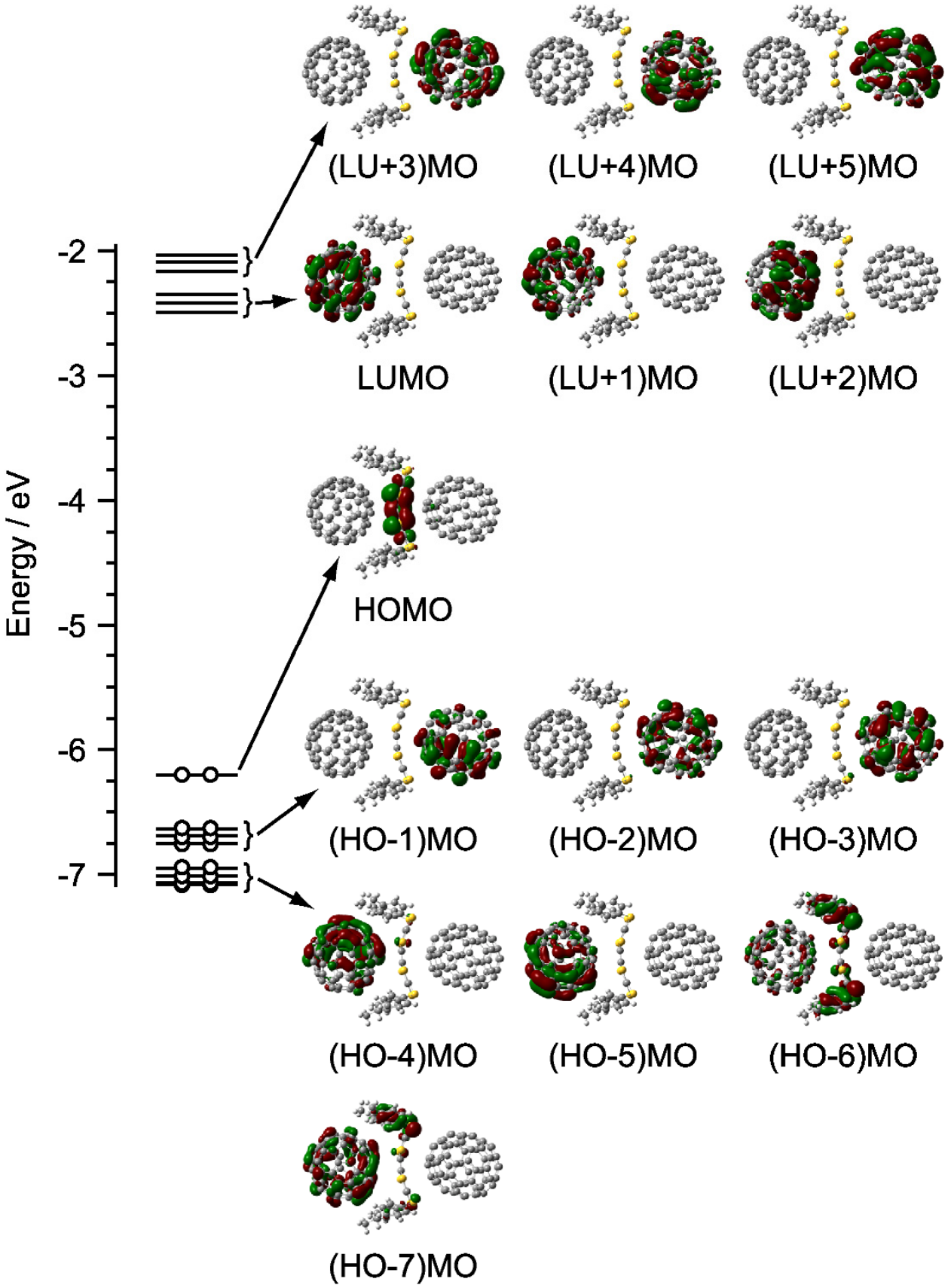

Fig. S28 Energy diagram of frontier Kohn-Sham orbitals for [C_{70}(L)-TTF3(A)-C_{70}(R)] cluster calculated at the CAM-B3LYP/6-31G(d,p) level of theory.

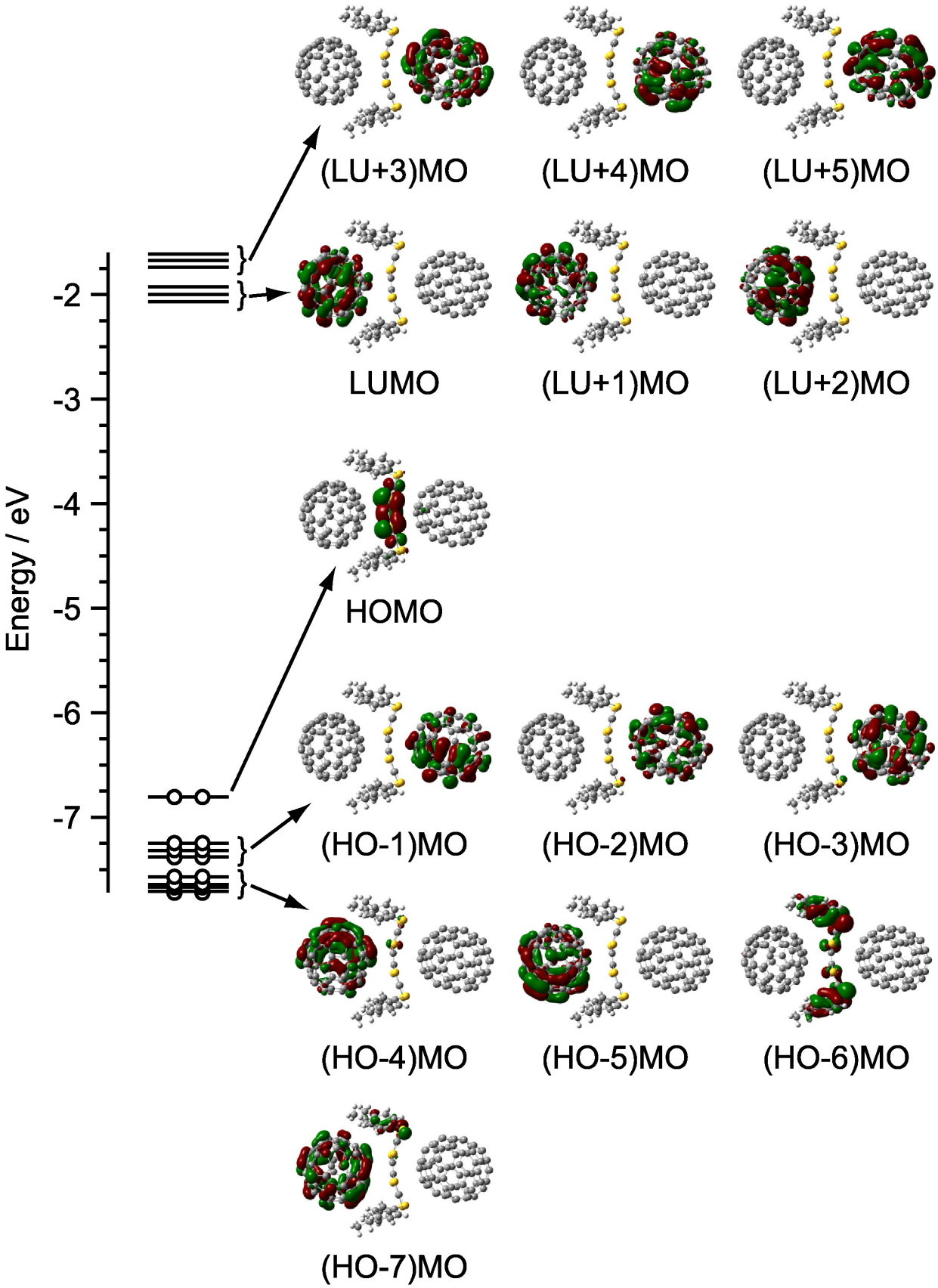

Fig. S29 Energy diagram of frontier Kohn-Sham orbitals for [C_{70}(L)-TTF3(A)-C_{70}(R)] cluster calculated at theωB97X-D/6-31G(d,p) level of theory.